Pergamon

Int. J. Heat Mass Transfer. Vol. 40, No. 10, pp. 2467–2475, 1997

0017-9310/97 $17.00+0.00

PII: S0017-9310(96)00316-X

Discrete-ordinate solutions for radiative transfer in a cylindrical enclosure with Fresnel boundaries

CHIH-YANG WU and BO-TING LIOU

Department of Mechanical Engineering, National Cheng Kung University, Tainan, Taiwan 701, Republic of China

(*Received* 22 *February* 1996 *and in final form* 21 *March* 1996)

Abstract—This work considers radiative heat transfer in a 2-D cylindrical scattering medium with Fresnel boundaries. The present analysis divides the radiative intensity into the attenuated incident and in-scattering components, solves the resulting problem of the former analytically, and that of the latter by the discrete-ordinate method (DOM). In addition, the present analysis rationalizes the distribution of the quadrature points used by the DOM to treat relevantly the strongly angular dependence of radiative intensity around the critical angles. Comparisons of the results obtained by the different methods show that the above techniques can improve the discrete-ordinate solutions. The present results reveal that the gradient of radiative heat flux in a cylindrical medium with Fresnel boundaries may vary abruptly at some locations.

1. INTRODUCTION

Since Chandrasekhar [1] and Lathrop [2] pioneered the discrete-ordinate method (DOM), and then Fiveland [3] applied the DOM to multi-dimensional radiative heat transfer, the DOM has become one of the most popular methods in the heat transfer community for solving radiative transfer problems involving scattering. This is because: (i) the DOM can be carried out to a high order and accuracy, (ii) the derivation of DOM schemes is relatively simple, and (iii) the DOM is compatible with the finite-difference or finite-element schemes for convective–diffusive transport phenomena. In multi-dimensional problems, the DOM suffers from the ray effects which arise from the approximation of the angular distribution of radiation by a set of discrete ordinates [4, 5]. Most researchers attribute the ray effects to the geometry. In practice, angularly dependent transmission and reflection, such as Fresnel reflection, may also cause ray effects, because the Fresnel reflection can also result in abrupt variations in the angular distribution of radiation. To remedy the ray effects, a new version of the DOM that rationalizes the distribution of the discrete ordinates has proved to be effective [6]. To apply the method, the integral over direction is split into integrals over several subintervals by the critical angle, and each subinterval uses a set of quadrature points. Through using the composite quadrature, the composite DOM (CDOM) can take the intensity within each subinterval adequately into account. In this work, the CDOM is further extended to solve multi-dimensional problems, where the geometry may also result in ray effects. Moreover, to remedy the ray effects due to the combination of geometry and Fresnel reflections, this work adopts a technique based on splitting radiation intensity into two parts. One of the two parts—the attenuated incident radiation—can be solved analytically, and its moments can be evaluated accurately. To demonstrate the aforementioned techniques for remedies of ray effects, this work considers radiative heat transfer in a 2-D cylindrical medium with Fresnel boundaries.

Recently, studies on almost every aspect of the DOM applied to multi-dimensional radiative heat transfer have been reported: the selection of discrete ordinates [7, 8], the improvement of spatial differencing schemes [9, 10], remedies for ray effects [4, 5], and applications to complex geometry [11, 12]. All of the above studies consider the reflectivities at the boundaries to be constant. However, in some engineering applications the angular dependence of reflectivity at boundaries may be important. Among these are optical windows, liquid optical filters and some solar collector devices. Therefore, this work aims at the improvement of the DOM for radiative heat transfer in a multi-dimensional medium with Fresnel boundaries. For the 2-D cylindrical problem considered, the effectiveness of the techniques proposed is examined, and the effects of the refractive index and the optical size are investigated.

2. ANALYSIS

Radiative heat transfer in an absorbing, isotropically scattering, 2-D cylindrical medium with

NOMENCLATURE

a	aspect ratio
I	radiation intensity or I_s in Section 3.2
I_a	attenuated incident radiation by absorption and out-scattering
I_d	intensity of the diffuse incident radiation
I_s	intensity caused by in-scattering
L_d	optical length defined in equation (12)
n	refractive index of the medium
N_r	maximum number of reflections
N_q	number of Gaussian quadrature points
q	normalized radiative flux
Q	total normalized axial heat transfer rate
S	source function
S_s	source function caused by in-scattering [equation (9)]
t	Gaussian quadrature points
w	Gaussian quadrature weights
$w_{n,m}$	product quadrature weights.

Greek symbols

$\Delta\tau_H$	optical distance between grid points in the axial direction
$\Delta\tau_R$	optical distance between grid points in the radial direction
θ	polar angle (Fig. 1)
θ_{g0}, θ_{g1}	polar angles defined in equations (11) and (13)
μ, ξ, η	directional cosines aligned with axial, radial and azimuthal axes, respectively
μ_0	directional cosine of incident angle
μ_c	directional cosine of critical angle θ_c
μ_{s0}, μ_{s1}	directional cosines of effective angles θ_{s0} and θ_{s1}, respectively
ρ	reflectivity of radiation incident on the surroundings from the medium
ρ_0	reflectivity for radiation incident on the medium from the surroundings
τ	optical coordinates
τ_H	optical size in the axial direction (Fig. 1)
τ_R	optical size in the radial direction (Fig. 1)
ϕ	azimuthal angle (Fig. 1)
ω	scattering albedo.

Subscripts

a	attentuation
m	discrete ordinate for ϕ
n	discrete ordinate for μ
r	r-direction
z	z-direction.

Superscripts

+, −	positive and negative directions of propagation.

constant properties is considered. The upper surface is exposed to uniform diffuse incident radiation. It is assumed that the emission from the medium and boundaries is negligible. A schematic diagram of the geometry and coordinates is shown in Fig. 1. The radiative transport equation can then be expressed as

$$\frac{\xi}{\tau_r}\frac{\partial}{\partial\tau_r}(\tau_r I)+\mu\frac{\partial I}{\partial\tau_z}-\frac{1}{\tau_r}\frac{\partial}{\partial\phi}(\eta I)+I=S$$
$$0\leqslant\tau_r\leqslant\tau_R \quad 0\leqslant\tau_z\leqslant\tau_H \qquad (1)$$
$$-1\leqslant\mu\leqslant 1 \quad 0\leqslant\phi\leqslant 2\pi$$

where I denotes the radiation intensity; ξ, η and μ the directional cosines defined by $\xi=\sin\theta\cos\phi$, $\eta=\sin\theta\sin\phi$ and $\mu=\cos\theta$, with θ and ϕ denoting the polar angle and the azimuthal angle, respectively; τ_r and τ_z the optical coordinates in the radial and axial directions, respectively, defined as the products of geometric coordinates and extinction coefficient of the medium; τ_R and τ_H the optical radius and height, respectively; and S the source function, defined as

$$S(\tau_r,\tau_z)=\frac{\omega}{4\pi}\int_{\phi'=0}^{2\pi}\int_{-1}^{1}I(\tau_r,\tau_z,\mu',\phi')\mathrm{d}\mu'\,\mathrm{d}\phi' \qquad (2)$$

where ω is the scattering albedo defined as the scattering coefficient divided by the extinction coefficient. The subscript υ, which denotes the spectrally dependent properties of the medium and boundaries, is omitted to simplify the mathematical expression.

Here, we consider the medium to be a dielectric material with its suspension of particulates, and the refractive indices of the upper and lower surroundings are assumed to be unity. The upper and lower interfaces are assumed to be optically smooth, so that the reflections and transmission are governed by Fresnel's equation and Snell's law. The side wall is assumed to be non-reflecting for simplicity of demonstration. If the lateral surroundings are opaque and black, the

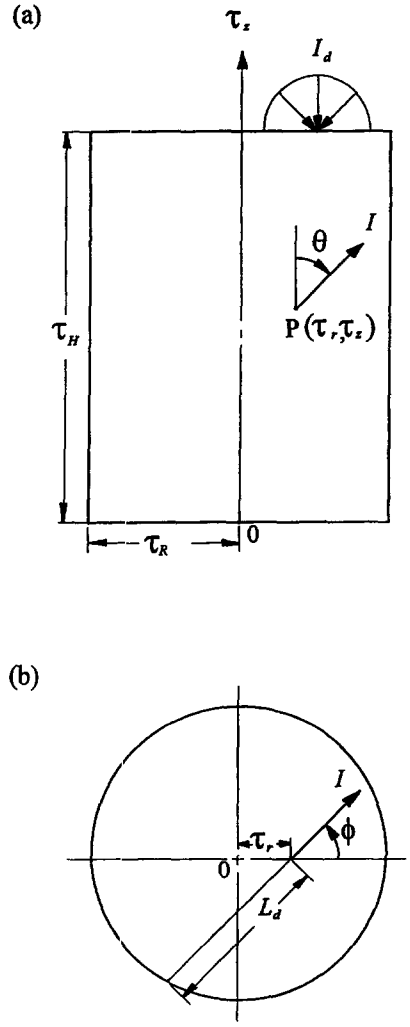

Fig. 1. Geometry and coordinates: (a) front view, (b) top view.

non-reflecting condition may hold. For example, either the bottom or side wall of a basin-type solar collector can be treated as a non-reflecting boundary. Hence, the boundary conditions can be expressed as

$$I(\tau_r, \tau_H, -\mu, \phi) = n^2 I_d[1-\rho_0(-\mu_0)] + \rho(\mu) I(\tau_r, \tau_H, \mu, \phi) \quad 0 \leqslant \tau_r \leqslant \tau_R \quad 0 \leqslant \mu \leqslant 1 \quad 0 \leqslant \phi \leqslant 2\pi \tag{3}$$

$$I(\tau_r, 0, \mu, \phi) = \rho(\mu) I(\tau_r, 0, -\mu, \phi) \quad 0 \leqslant \tau_r \leqslant \tau_R \quad 0 \leqslant \mu \leqslant 1 \quad 0 \leqslant \phi \leqslant 2\pi \tag{4}$$

$$I(\tau_R, \tau_z, \mu, \phi) = 0 \quad 0 \leqslant \tau_z \leqslant \tau_H \quad -1 \leqslant \mu \leqslant 1 \quad \pi/2 \leqslant \phi \leqslant 3\pi/2 \tag{5}$$

where n is the refractive index of the medium, I_d the intensity of the diffuse incident radiation, μ_0 the directional cosine of the incident angle in the surroundings, and ρ_0 and ρ the interface reflectivities for radiation incident on the medium from the surroundings and that for radiation incident on the surroundings from the medium, respectively. The value of the reflectivity is unity for $|\mu| < \mu_c$, where $\mu_c = \sqrt{1-1/n^2}$ is the directional cosine of the critical angle.

Since equations (1)–(5) are linear, the problem can be readily split into two simpler problems [13–15] by dividing the intensity into two components, I_a and I_s; that is

$$I(\tau_r, \tau_z, \mu, \phi) = I_a(\tau_r, \tau_z, \mu, \phi) + I_s(\tau_r, \tau_z, \mu, \phi). \tag{6}$$

Physically, I_a is the attenuated incident radiation by absorption and out-scattering, and I_s is caused by in-scattering. Here, the governing equation for I_a can be expressed as

$$\frac{\xi}{\tau_r}\frac{\partial}{\partial \tau_r}(\tau_r I_a) + \mu \frac{\partial I_a}{\partial \tau_z} - \frac{1}{\tau_r}\frac{\partial}{\partial \phi}(\eta I_a) + I_a = 0 \tag{7}$$

and the boundary conditions for I_a are the same as in equations (3)–(5) except for replacing I with I_a. The above problem for I_a can be solved analytically. Subtracting equation (7) from equations (1) and (2), we obtain the governing equation for I_s expressed as

$$\frac{\xi}{\tau_r}\frac{\partial}{\partial \tau_r}(\tau_r I_s) + \mu \frac{\partial I_s}{\partial \tau_z} - \frac{1}{\tau_r}\frac{\partial}{\partial \phi}(\eta I_s) + I_s = S = S_s + S_a \quad 0 \leqslant \tau_r \leqslant \tau_R \quad 0 \leqslant \tau_z \leqslant \tau_H \quad -1 \leqslant \mu \leqslant 1 \quad 0 \leqslant \phi \leqslant 2\pi \tag{8}$$

where

$$S_s(\tau_r, \tau_z) = \frac{\omega}{4\pi}\int_{\phi'=0}^{2\pi}\int_{-1}^{1} I_s(\tau_r, \tau_z, \mu', \phi')\,d\mu'\,d\phi' \tag{9}$$

$$S_a(\tau_r, \tau_z) = \frac{\omega}{4\pi}\int_{\phi'=0}^{2\pi}\int_{-1}^{1} I_a(\tau_r, \tau_z, \mu', \phi')\,d\mu'\,d\phi'. \tag{10}$$

The boundary conditions for I_s are also the same as in equations (3)–(5) except for replacing I with I_s and removing the incident term [i.e. the first term on the right-hand side of equation (3)].

Exact solution of the problem for I_a and the associated accurate calculation for the moments of I_a, such as S_a, are crucial for the discrete-ordinate solutions of a multi-dimensional transfer problem. Either the ray-tracing technique or the image method [16] can be applied to treat the Fresnel reflections at the upper and lower interfaces, which yield an infinite number of images in the τ_z-direction, as shown in Fig. 2. Similar to the evaluation of specular view factors, the calculation of the attenuated part of the incident radiation, I_a, must take the contribution for each possible direct or reflection path into account. The path may be traced back to each possible entry point where the external radiation enters the medium, and I_a with

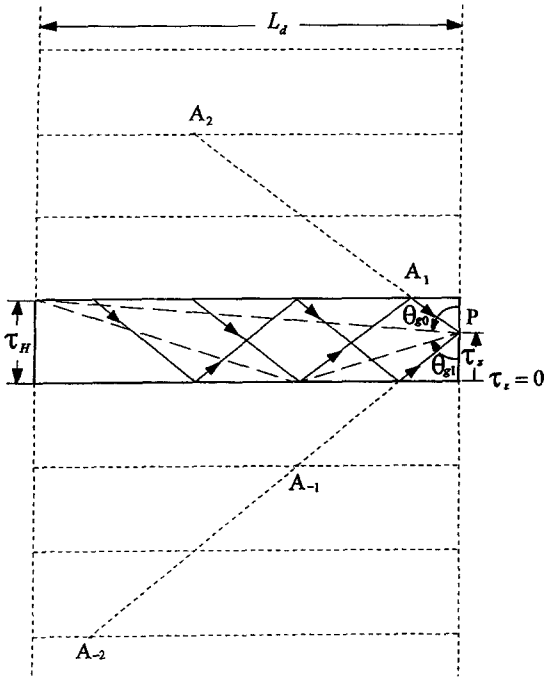

Fig. 2. Cross section of a medium with images at specified τ_r and ϕ.

reflections may be treated as that from the images of an entry point to the point considered, as shown in Fig. 2. If $n = 1.0$, the intensity I_a appears only within $\pi - \theta_{g0} \leqslant \theta \leqslant \pi$. From geometric relations, θ_{g0} can be expressed as

$$\theta_{g0}(\tau_r, \tau_z, \phi) = \tan^{-1}[L_d/(\tau_H - \tau_z)] \tag{11}$$

where

$$L_d = \sqrt{\tau_R^2 - \tau_r^2 \sin^2\phi} + \tau_r \cos\phi. \tag{12}$$

Furthermore, if $n \neq 1.0$, the intensity arriving is limited within the critical angle θ_c, because of the refraction at the interface. Therefore, if $n \neq 1.0$, the intensity I_a with $\mu < 0$ appears within $\pi - \theta_{s0} \leqslant \theta \leqslant \pi$, where θ_{s0} is the effective angle defined as $\theta_{s0} = \min(\theta_{g0}, \theta_c)$, and the intensity I_a with $\mu > 0$ appears within $0 \leqslant \theta \leqslant \theta_{s1}$, where θ_{s1} is the effective angle defined as $\theta_{s1} = \min(\theta_{g1}, \theta_c)$, with

$$\theta_{g1}(\tau_r, \tau_z, \phi) = \tan^{-1}[L_d/(\tau_H + \tau_z)]. \tag{13}$$

The contribution of radiation from each entry point is equal to the incident intensity multiplied by the interface transmissivity, the interface reflectivity of every reflection, and an exponential decay term due to extinction over the traveling optical distance. Thus, the intensity along a ray path may be expressed as a sum of the contributions of the incident intensity at each entry point on the ray path. For the present case, the reflection may not be infinite because of the non-reflecting side wall, except for $\theta_0 = \pi$. Therefore, the intensity $I_a(\tau_r, \tau_z, \mu, \phi)$ can be expressed as

$$I_a(\tau_r, \tau_z, \mu, \phi) = I_d n^2 [1 - \rho_0(-\mu_0)]\rho(\mu) e^{-(\tau_H + \tau_z)/\mu} \times \frac{1 - [\rho^2(\mu) e^{-2\tau_H/\mu}]^{(N_r+1)/2}}{1 - \rho^2(\mu) e^{-2\tau_H/\mu}} \quad \mu_{s1}(\phi) \leqslant \mu \leqslant 1 \tag{14}$$

$$I_a(\tau_r, \tau_z, \mu, \phi) = I_d n^2 [1 - \rho_0(-\mu_0)] e^{(\tau_H - \tau_z)/\mu} \times \frac{1 - [\rho^2(|\mu|) e^{2\tau_H/\mu}]^{N_r/2+1}}{1 - \rho^2(|\mu|) e^{2\tau_H/\mu}} \quad -1 \leqslant \mu \leqslant -\mu_{s0}(\phi) \tag{15}$$

where N_r is the maximum number of reflections determined by

$$N_r = 1 + 2\left\lceil \frac{L_d - (\tau_H + \tau_z)\tan\theta}{2\tau_H \tan\theta} \right\rceil \quad \mu_{s1}(\phi) \leqslant \mu \leqslant 1 \tag{16}$$

$$N_r = 2\left\lceil \frac{L_d - (\tau_H - \tau_z)|\tan\theta|}{2\tau_H |\tan\theta|} \right\rceil \quad -1 \leqslant \mu \leqslant -\mu_{s0}(\phi). \tag{17}$$

Here, the operator $\lceil \cdot \rceil$ in equations (16) and (17) means taking the greatest integer less or equal to the operated value. If there are no specular reflections on the boundaries, $N_r = 0$. Thus, $N_r = 0$ for a medium with $n = 1.0$.

3. NUMERICAL SOLUTION

3.1. *Calculation for* S_a

Using the DOM, we approximate the moments of intensity over a full or half range by the weighted sums of the intensity at a set of discrete ordinates. When the distribution of radiation intensity over direction has a discontinuity or abrupt variation, the ray effect causes serious errors. It is worth noting that splitting the angular range into several subintervals with continuous distributions of intensity, and applying one set of quadrature points to the integration over each of the subintervals can improve the results [6]. Thus, we may expect that applying such a splitting technique to the evaluation of S_a and other moments of intensity can remedy the ray effect and improve discrete-ordinate solutions.

The geometry of the medium and the refraction of the incoming radiation result in the discontinuous distribution or abrupt variation of intensity I_a at $\pi - \theta_{s0}$ and θ_{s1}. In addition, the two factors and the multiple specular reflections at the upper and lower interfaces result in more abrupt variations of intensity over directions. Fortunately, the abrupt variations due to multiple reflections are minor because of the exponential decay of I_a. Therefore, we consider only the abrupt variations of intensity at $\pi - \theta_{s0}$ and θ_{s1}, and apply a set of Gaussian quadrature points to each of the two effective ranges $\pi - \theta_{s0} \leqslant \theta \leqslant \pi$ and

$0 \leqslant \theta \leqslant \theta_{s1}$. The Gaussian quadrature is adopted, because it can generate highly accurate results.

Because of the symmetry characteristics, it is sufficient to consider just $(0, \pi)$ in the ϕ-direction. The ϕ-direction is split into two subintervals, $(0, \pi/2)$ and $(\pi/2, \pi)$, and then each subinterval uses a set of Gaussian quadrature points. The Gaussian quadrature points used in each subinterval of θ and ϕ are the same. Therefore, the discrete-ordinate formulation of equation (10) expressed in product formula is written as

$$S_a(\tau_r, \tau_z) = \frac{\omega}{16} \sum_{m=1}^{2N_q} w_m \sum_{n=1}^{N_q} w_n \times \{[1-\mu_{s0}(\phi_m)] I_a[\tau_r, \tau_z, \mu_n^-(\phi_m), \phi_m] + [1-\mu_{s1}(\phi_m)] I_a[\tau_r, \tau_z, \mu_n^+(\phi_m), \phi_m]\} \quad (18)$$

where

$$\phi_m = (\pi t_m + \pi)/4 \quad \text{for } m = 1, \ldots, N_q \quad (19)$$

$$\phi_m = \pi/2 + \phi_{m-N_q} \quad \text{for } m = N_q+1, \ldots, 2N_q \quad (20)$$

$$\mu_n^-(\phi_m) = -\{[1-\mu_{s0}(\phi_m)] t_n + \mu_{s0}(\phi_m) + 1\}/2 \quad \text{for } n = 1, \ldots, N_q \quad (21)$$

$$\mu_n^+(\phi_m) = \{[1-\mu_{s1}(\phi_m)] t_n + \mu_{s1}(\phi_m) + 1\}/2 \quad \text{for } n = 1, \ldots, N_q. \quad (22)$$

Here, the subscripts m and n represent the discrete ordinates for ϕ and μ, respectively; N_q is the number of Gaussian quadrature points; w denotes the quadrature weights corresponding to the Gaussian quadrature points t; and $\mu_{s0}(\phi_m)$ and $\mu_{s1}(\phi_m)$ are the directional cosines of the effective angles on the plane with $\phi = \phi_m$. The other moments of I_a will be calculated in a similar way.

3.2. *Discrete-ordinate form*

We now extend the CDOM [6] technique to a 2-D cylindrical problem with Fresnel boundaries. The product formula seems to be straightforward for a 2-D problem. The integral over $(-1, 1)$ for μ is split into integrals over several subintervals: $(-1, -\mu_c)$, $(-\mu_c, \mu_c)$ and $(\mu_c, 1)$. The integral over the ϕ-direction is split into two subintervals: $(0, \pi/2)$ and $(\pi/2, \pi)$. The integral over each subinterval uses a set of Gaussian quadrature points.

By omitting the subscript s of I_s, the discrete-ordinate representation of equation (8) can be written as

$$\frac{\xi_{n,m}}{\tau_r} \frac{\partial}{\partial \tau_r}(\tau_r, I_{n,m}) + \mu_n \frac{\partial I_{n,m}}{\partial \tau_z} - \frac{1}{\tau_r} \frac{\partial}{\partial \phi}(\eta_{n,m} I_{n,m}) + I_{n,m} = S \quad 0 \leqslant \tau_r \leqslant \tau_R \quad 0 \leqslant \tau_z \leqslant \tau_H \quad n = 1, \ldots, 3N_q \quad m = 1, \ldots, 2N_q \quad (23)$$

where

$$S = S_a + \frac{\omega}{4\pi} \sum_{m'=1}^{2N_q} \sum_{n'=1}^{3N_q} w_{n',m'} I_{n',m'} \quad (24)$$

with

$$w_{n',m'} = \frac{\pi}{4}(1-\mu_c) w_{n'} w_{m'} \quad \text{for } n = 1, \ldots, N_q, \; 2N_q+1, \ldots, 3N_q \text{ and } m = 1, \ldots, 2N_q \quad (25)$$

$$w_{n',m'} = \frac{\pi}{2} \mu_c w_{n'} w_{m'} \quad \text{for } n = N_q+1, \ldots, 2N_q \text{ and } m = 1, \ldots, 2N_q \quad (26)$$

where S_a is generated by equation (18). The boundary conditions are expressed in a discretized form as

$$I_{3N_q/2+n,m} = \rho(|\mu_{3N_q/2+n}|) I_{3N_q/2+1-n,m} \quad \mu_{3N_q/2+n} < 0 \quad \tau_z = \tau_H \quad (27)$$

$$I_{n,m} = \rho(\mu_n) I_{3N_q+1-n,m} \quad \mu_n > 0 \quad \tau_z = 0 \quad (28)$$

$$I_{n,m} = I_{n,m'} \quad \xi_{n,m} > 0 \quad \xi_{n,m'} < 0 \quad \tau_r = 0 \quad (29)$$

$$I_{n,N_q+m} = 0 \quad \xi_{n,N_q+m} < 0 \quad \tau_r = \tau_R. \quad (30)$$

Applying the weighted diamond differencing scheme to the spatial derivatives in equation (23), the final discretization equations can be written for each sweep direction. Details of the theory and solution technique are available in ref. [17]. The solutions can be performed iteratively by sweeping through each direction with the boundary conditions, equations (27)–(30). The iterative procedure is continued until the maximum relative difference between two successive calculations of incident radiation at each cell center is less than 1×10^{-6}.

After determining the intensity, we can obtain the radiative fluxes just leaving the upper surface, $q_z^+(\tau_r, \tau_H)$, just leaving the lower surface, $q_z^-(\tau_r, 0)$, toward the side wall $q_r^+(\tau_R, \tau_z)$, and the net axial radiative fluxes in the medium, $q_z(\tau_r, \tau_z)$, from their quadrature approximations

$$q_z^+(\tau_r, \tau_H) = \sum_{n=1}^{N_q} w_n \rho_0 \left(\frac{t_n+1}{2}\right)\left(\frac{t_n+1}{2}\right) + \frac{1}{4I_d} \sum_{m=1}^{2N_q} w_m \sum_{n=1}^{N_q} w_n \Big\langle [1-\mu_{s1}(\phi_m)] \times I_a[\tau_r, \tau_H, \mu_n^+(\phi_m), \phi_m] \times \{1-\rho[\mu_n^+(\phi_m)]\} \mu_n^+(\phi_m) \Big\rangle + \frac{1}{\pi I_d} \sum_{m=1}^{2N_q} \sum_{n=1}^{3N_q/2} w_{n,m} [1-\rho(\mu_n)] I_{n,m}(\tau_r, \tau_H) \mu_n \quad (31)$$

$$q_z^-(\tau_r,0) = -\frac{1}{4I_d}\sum_{m=1}^{2N_q} w_m \sum_{n=1}^{N_q} w_n \times \Big\langle [1-\mu_{s0}(\phi_m)]I_a[\tau_r,0,\mu_n^-(\phi_m),\phi_m] \times \{1-\rho[|\mu_n^-(\phi_m)|]\}\mu_n^-(\phi_m)\Big\rangle - \frac{1}{\pi I_d}\sum_{m=1}^{2N_q} \times \sum_{n=3N_q/2+1}^{3N_q} w_{n,m}[1-\rho(|\mu_n|)]I_{n,m}(\tau_r,0)\mu_n \quad (32)$$

$$q_r^+(\tau_R,\tau_z) = \frac{1}{4I_d}\sum_{m=1}^{N_q} w_m \cos\phi_m \sum_{n=1}^{N_q} w_n \times \Big\{[1-\mu_{s0}(\phi_m)]I_a[\tau_R,\tau_z,\mu_n^-(\phi_m),\phi_m] \times \sqrt{1-[\mu_n^-(\phi_m)]^2} + [1-\mu_{s1}(\phi_m)] \times I_a[\tau_R,\tau_z,\mu_n^+(\phi_m),\phi_m] \times \sqrt{1-[\mu_n^+(\phi_m)]^2}\Big\} + \frac{1}{\pi I_d}\sum_{m=1}^{N_q} \times \sum_{n=1}^{3N_q} w_{n,m}I_{n,m}(\tau_R,\tau_z,)\xi_{n,m} \quad (33)$$

$$q_z(\tau_r,\tau_z) = \frac{1}{4I_d}\sum_{m=1}^{2N_q} w_m \sum_{n=1}^{N_q} w_n \times \{[1-\mu_{s0}(\phi_m)]I_a[\tau_r,\tau_z,\mu_n^-(\phi_m),\phi_m]\mu_n^-(\phi_m) + [1-\mu_{s1}(\phi_m)]I_a[\tau_r,\tau_z,\mu_n^+(\phi_m),\phi_m]\mu_n^+(\phi_m)\} + \frac{1}{\pi I_d}\sum_{m=1}^{2N_q}\sum_{n=1}^{3N_q} w_{n,m}I_{n,m}(\tau_r,\tau_z)\mu_n. \quad (34)$$

The above quantities are normalized by πI_d. The first term on the right-hand side of equation (31) is the direct reflected portion of the external incident radiation.

4. RESULTS AND DISCUSSION

To examine the validity of the DOM using the product formula, a special case with $n = 1.0$ and $a = 1.0$, where a is the aspect ratio defined as $a = 2\tau_R/\tau_H$, is considered. The DOM results are obtained by using the product formula with $N_q = 2$ in each of the two subintervals, $(-1,0)$ and $(0,1)$, and by using discrete ordinates for the S_6-approximation [18]. Comparisons of the results with different grid sizes and quadrature orders show that the following choice is valid for this problem: (a) $\Delta\tau_R = \Delta\tau_H = 0.001$ for $\tau_R = 0.01$, (b) $\Delta\tau_R = \Delta\tau_H = 0.01$ for $\tau_R = 0.1$, (c) $\Delta\tau_R = \Delta\tau_H = 0.025$ for $0.1 < \tau_R < 0.5$, (d) $\Delta\tau_R = \Delta\tau_H = 0.05$ for $0.5 \leqslant \tau_R < 1.5$, (e) $\Delta\tau_R = \Delta\tau_H = 0.1$ for $\tau_R \geqslant 1.5$. In addition, except for additional mentions, the intensity is divided into I_a and I_s in the computation

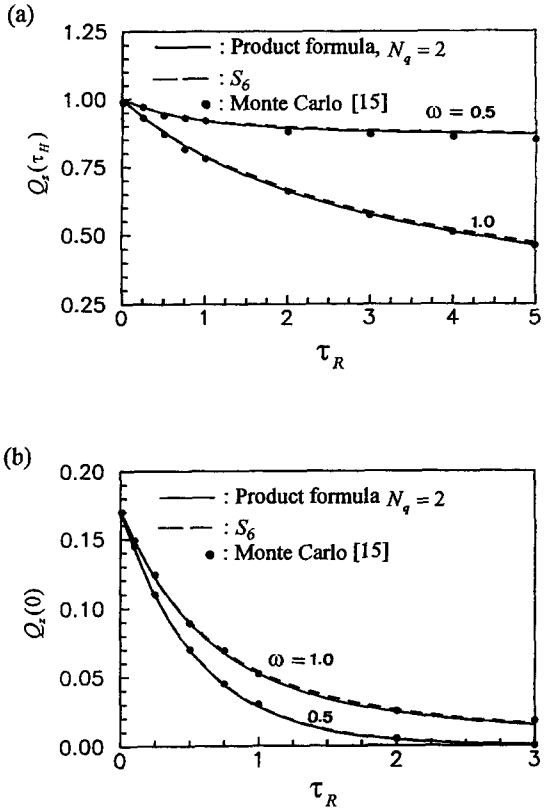

Fig. 3. Effect of τ_R and ω for $a = 1.0$ on the total normalized axial heat transfer rate: (a) at upper surface, (b) at lower surface.

performed. Figure 3(a) and (b) shows the total normalized axial heat transfer rates for the upper surface, $Q_z(\tau_H)$, and the lower surface, $Q_z(0)$, respectively, for various scattering albedos. $Q_z(\tau_H)$ and $Q_z(0)$ are determined from

$$Q_z(\tau_H) = 1 - \frac{2}{\tau_R^2}\int_0^{\tau_R} q_z^+(\tau_r,\tau_H)\tau_r\,d\tau_r, \quad (35)$$

$$Q_z(0) = \frac{2}{\tau_R^2}\int_0^{\tau_R} q_z^-(\tau_r,0)\tau_r\,d\tau_r. \quad (36)$$

As seen from Fig. 3(a) and (b), the results obtained by both versions of DOM are very close to those by the Monte Carlo method [15].

Table 1 shows that the solutions obtained by three DOM schemes, including the DOM using S_N discrete ordinates, the double DOM using the product formula and two subintervals, $(-1,0)$ and $(0,1)$, and the CDOM using the product formula and three subintervals, $(-1,-\mu_c)$, $(-\mu_c,\mu_c)$ and $(\mu_c,1)$. The three schemes use $\Delta\tau_R = \Delta\tau_H = 0.05$. Comparisons of the results shown in Table 1 indicate that the 2-D solutions with $a = 30$ are close to the 1-D solutions [19]. Moreover, the results obtained by the CDOM using the product formula and three subintervals monotonically approach those of the 1-D planar, as N_q increases, and the accuracy of the CDOM even using

Table 1. Comparison of results generated by the three schemes for $\tau_H = 1.0$, $a = 30$ and $n = 1.5$ with those of the 1-D planar [19]: S_N approximation (a), product formula with two subintervals for μ (b), and that with three subintervals for μ (c)

(a)	$\omega = 1.0$		$\omega = 0.5$	
S_N	$q_z^+(0,\tau_H)$	$q_z^-(0,0)$	$q_z^+(0,\tau_H)$	$q_z^-(0,0)$
S_4	0.41339	0.59023	0.15125	0.34038
S_6	0.40171	0.59225	0.11522	0.30967
S_8	0.41070	0.59267	0.13639	0.32761
1-D [19]	0.42033	0.57967	0.13909	0.30695
(b)	$\omega = 1.0$		$\omega = 0.5$	
N_q	$q_z^+(0,\tau_H)$	$q_z^-(0,0)$	$q_z^+(0,\tau_H)$	$q_z^-(0,0)$
3	0.42117	0.57850	0.14440	0.31152
5	0.42219	0.57759	0.14967	0.31601
8	0.42121	0.57850	0.14522	0.31228
1-D [19]	0.42033	0.57967	0.13909	0.30695
(c)	$\omega = 1.0$		$\omega = 0.5$	
N_q	$q_z^+(0,\tau_H)$	$q_z^-(0,0)$	$q_z^+(0,\tau_H)$	$q_z^-(0,0)$
2	0.41914	0.58042	0.13957	0.30770
4	0.41979	0.57975	0.13922	0.30719
6	0.41997	0.57957	0.13914	0.30707
1-D [19]	0.42033	0.57967	0.13909	0.30695

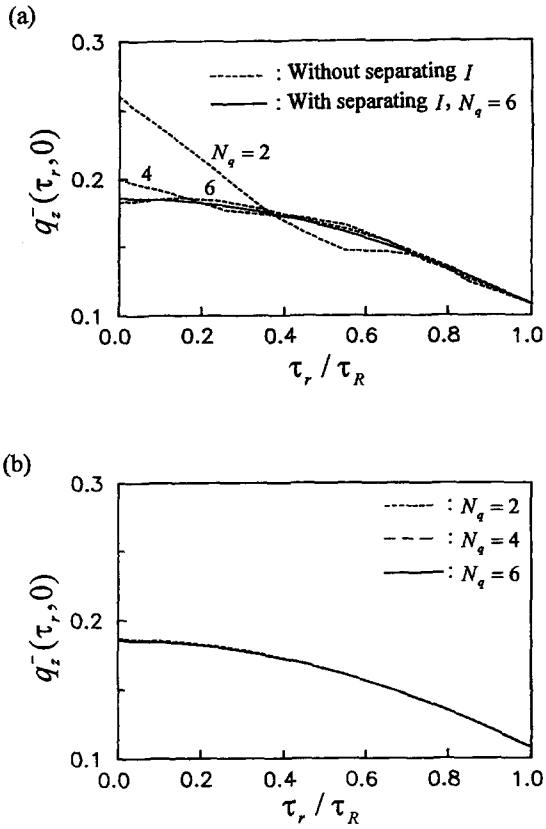

Fig. 4. Comparison of solutions for various orders of N_q, $\tau_H = 1.0$, $a = 1.0$, $\omega = 1.0$ and $n = 1.5$: (a) without separating I, (b) after separating I.

$N_q = 2$ is better than that of other schemes with higher quadrature orders.

Next, we examine the effectiveness of separating I into I_a and I_s. The results obtained by the CDOM without separating I are compared with those obtained by the CDOM after separating I by using $N_q = 6$, as shown in Fig. 4(a). The results shown are obtained by using $\Delta\tau_R = \Delta\tau_H = 0.05$. As expected, the results obtained without separating I oscillate about those obtained after separating I. When N_q increases, the frequency of the oscillations becomes higher and the magnitude becomes smaller. In addition, the results obtained after separating I for $N_q = 2$, 4 and 6 almost overlap each other, as shown in Fig. 4(b). The CPU time required to obtain the results for $N_q = 2$, 4 and 6 by using the scheme with separating I is about 6.1, 47.7 and 188.4 s, respectively, on a HP 715/64 workstation. It is worth noting that the CPU time required to obtain the results without separating I by using $N_q = 2$, 4 and 6 is about 4.4, 64.3 and 361.6 s, respectively. Consequently, it is effective to remedy the ray effects from CDOM by dividing I into two components and accurately calculating the moments of I_a.

Now, we turn to investigate the effects of the refractive index n and the aspect ratio a. The results shown in Figs. 5 and 6 for $\omega = 1.0$ and $\tau_R = 0.5$ are obtained by the CDOM using $N_q = 2$ and $\Delta\tau_R = \Delta\tau_H = 0.02$. n determines the interface reflectivity and transmissivity at the upper and lower boundaries; the combination of n and a determines the effective angles of I_a. Figure 5(a) and (b) shows the variation of $-q_z(0,\tau_z)$ and $q_r^+(\tau_R,\tau_z)$ with respect to τ_z. Although multiple internal reflections in a medium with $n > 1.0$ make the variation of $-q_z(0,\tau_z)$ and $q_r^+(\tau_R,\tau_z)$ even, the effective angle $\theta_{s0} = \min(\theta_{g0}, \theta_c)$ changes from θ_{g0} to θ_c at a certain location. Thus, there is a kink at the location, where θ_{s0} changes from θ_{g0} to θ_c in each of the curves of $-q_z(0,\tau_z)$ for $n = 1.5$ and 2.0 with $a = 0.2$ and 1.0, as shown in Fig. 5(a). This change of θ_{s0} represents an abrupt variation of the contribution of the external incident to $-q_z(0,\tau_z)$. For $a = 5.0$, θ_{s0} is equal to θ_c at any location on the axis for $n = 1.5$ and 2.0, and so there is no kink on their curves. The effect of internal reflections increases as n increases. Figure 5(b) shows that the $q_r^+(\tau_R,\tau_z)$ increases, as τ_z increases, and reaches the maximum at the upper surface, where external radiation enters the medium. Moreover, Fig. 5(b) indicates that the $q_r^+(\tau_R,\tau_z)$ near the upper surface for the medium with $n = 1.0$ is much greater than that for the other two media. This is because, for a medium with $n = 1.0$, θ_{s0} is always equal to θ_{g0} and is much greater than $\theta_{s0} = \theta_c$ for the two media with $n = 1.5$ and 2.0 as τ_z is greater than a certain value determined by n and a.

Figure 6(a) shows that $q_z^+(\tau_r,\tau_H)$ increases with the decrease in a for a medium with $n = 1.0$. This is

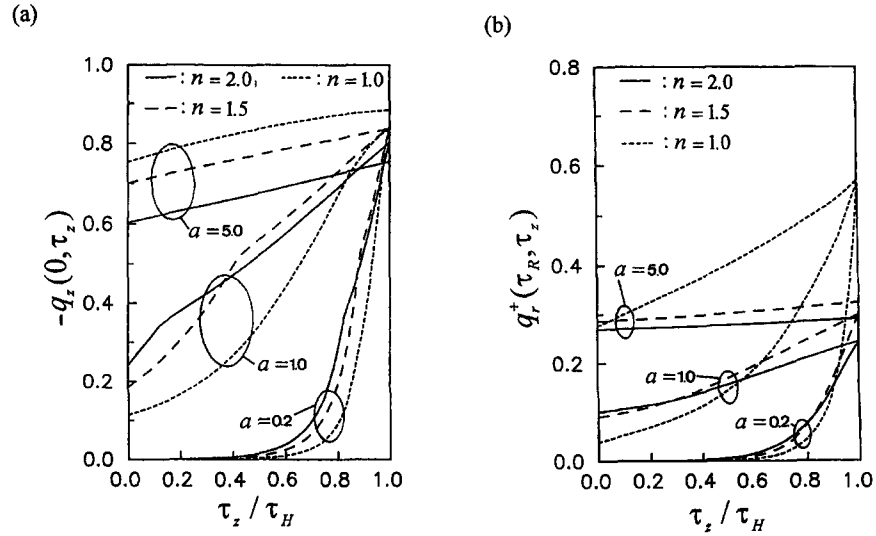

Fig. 5. Effects of n and a on the radiative fluxes for $\tau_R = 0.5$ and $\omega = 1.0$: (a) $-q_z(0,\tau_z)$, (b) $q_r^+(\tau_R,\tau_z)$.

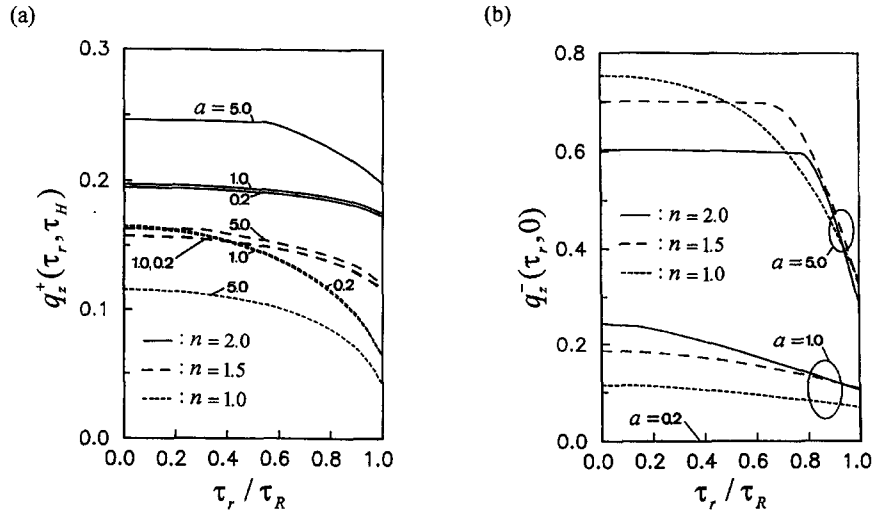

Fig. 6. Effects of n and a on the radiative fluxes for $\tau_R = 0.5$ and $\omega = 1.0$: (a) $q_z^+(\tau_r,\tau_H)$, (b) $q_z^-(\tau_r,0)$.

because $q_z^+(\tau_r,\tau_H)$ resulting purely from multiple scattering increases with the increase in the optical thickness for a medium with $n = 1.0$. The results for $n = 1.5$ and 2.0 do not show the same tendency, since both multiple scattering and multiple internal reflections contribute to $q_z^+(\tau_r,\tau_H)$. In addition, since the contribution of the direct reflection of the external incident radiation dominates $q_z^+(\tau_r,\tau_H)$ for $n = 1.5$ and 2.0 and increases with n, $q_z^+(\tau_r,\tau_H)$ for $n = 2.0$ is larger than for $n = 1.5$, as shown in Fig. 6(a).

Figure 6(b) indicates that $q_z^-(\tau_r,0)$ decreases with the decrease in a. The values of $q_z^-(\tau_r,0)$ approach zero for the cases with $a = 0.2$. This is because most of the radiation is scattered out of the side wall of a tall cylinder before reaching the lower surface. We then examine the curves of $q_z^-(\tau_r,0)$ for $a = 5.0$. For locations around the axis, $\theta_{s0} = \theta_{g0}$ in a medium with $n = 1.0$ is much greater than $\theta_{s0} = \theta_c$ in a medium with $n = 1.5$ or 2.0. Although I_a is proportional to n^2, the total contribution of I_a over the effective angle to radiative transfer in a medium with $n = 1.5$ or 2.0 is less than that to radiative transfer in a medium with $n = 1.0$. Thus, $q_z^-(\tau_r,0)$ decreases with the increase in n. However, when τ_r becomes large, $\theta_{s0} = \theta_{g0}$ in a medium with $n = 1.0$ is not much greater than $\theta_{s0} = \theta_c$ in a medium with $n = 1.5$ or 2.0. Thus, the $q_z^- - \tau_r$ curve for $n = 1.0$ crosses over that for $n = 1.5$ or 2.0, as shown in Fig. 6(b). As for $a = 1.0$, the values of $q_z^-(\tau_r,0)$ increase with n, except at locations very close to the side wall. The reasons are similar to those for the curves for $a = 5.0$. Moreover, large variations in the slopes of the $q_z - \tau_r$ curves appear for $n = 1.5$ and 2.0, as shown in Fig. 6(b). This is due to the abrupt change in θ_{s0} from θ_c to θ_{g0}, where θ_c depends on n and θ_{g0} depends on ϕ, a and τ_r. This tendency is significant for an optically thin case ($a = 5.0$).

5. CONCLUSIONS

This work considers radiative heat transfer in a 2-D cylindrical participating medium with Fresnel boundaries. The geometry of the medium and the interface transmissivity at Fresnel boundaries result in a discontinuity or an abrupt variation in the distribution of radiative intensity over directions. To remedy the ray effects, the present analysis divides the radiative intensity into the attenuated incident and in-scattering components, solves the resulting problem of the former analytically, and that of the latter by the CDOM. Based on the comparisons of the results obtained by different methods, it is shown that the above techniques can improve the discrete-ordinate solutions. The present results reveal that the radiative heat flux in a cylindrical medium with Fresnel boundaries may have abrupt variations in slope at some locations. Those locations depend on the refractive index and geometry.

REFERENCES

1. Chandrasekhar, S., *Radiative Transfer*, Chap. 2. Clarendon Press, Oxford, 1950.
2. Lathrop, K. D., Use of discrete-ordinates methods for solution of photon transport problems. *Nuclear Science and Engineering*, 1966, **24,** 381–388.
3. Fiveland, W. A.. A discrete ordinates method for predicting radiation heat transfer in axisymmetric enclosures. ASME Paper 82-HT-20, 1982.
4. Chai, J. C., Lee, H. S. and Patankar, S. V., Ray effect and false scattering in the discrete ordinates method, *Numerical Heat Transfer*, 1993, **B24,** 373–389.
5. Pasini, S. and Castellano, L., Numerical experiments on the application of the diamond scheme to sets of discrete directions obtained from a random numbers generator. ASME-HTD, 1994, Vol. 276, pp. 99–104.
6. Wu, C.-Y., Liou, B.-T. and Liou, J.-H., Discrete-ordinate solutions for radiative transfer in a scattering medium with Fresnel boundaries. In *Proceedings of the Tenth International Heat Transfer Conference*, Vol. 2, Taylor & Francis, Bristol, PA, 1994, pp. 159–164.
7. Koch, R., Krebs, W., Wittig, S. and Viskanta, R., Discrete ordinates quadrature schemes for multidimensional radiative transfer. *Journal of Quantitative Spectroscopy & Radiative Transfer*, 1995, **53,** 353–372.
8. Thurgood, C. P., Pollard, A. and Becker, H. A., The T_N quadrature set for the discrete ordinates method. *Journal of Heat Transfer*, 1995, **117,** 1068–1070.
9. Chai, J. C., Lee, H. S. and Patankar, S. V., Evaluation of spatial differencing practices for the discrete-ordinates method. *Journal of Thermophysics*, 1994, **8,** 140–144.
10. Chai, J. C., Lee, H. S. and Patankar, S. V., Improved treatment of scattering using the discrete ordinates method. *Journal of Heat Transfer*, 1994, **116,** 260–263.
11. Fiveland, W. A. and Jessee, J. P., A finite element formulation of the discrete-ordinates method for multidimensional geometries. *Journal of Thermophysics*, 1995, **9,** 47–54.
12. Chai, J. C., Parthasarathy, G., Lee, H. S. and Patankar, S. V., Finite volume radiative heat transfer procedure for irregular geometries. *Journal of Thermophysics*, 1995, **9,** 410–415.
13. Olfe, D. B., A modification of differential approximation for radiative transfer. *AIAA Journal*, 1967, **5,** 638–643.
14. Wu, C. Y., Sutton, W. H. and Love, T. J., Successive improvement of the modified differential approximation in radiative heat transfer. *Journal of Thermophysics*, 1987, **1,** 296–300.
15. Modest, M. F., Modified differential approximation for radiative transfer in general three-dimensional media. *Journal of Thermophysics*, 1989, **3,** 283–288.
16. Wu, C.-Y., Integral equations for radiative transfer with linear anisotropic scattering and Fresnel boundaries. *Journal of Thermophysics*, 1988, **3,** 68–74.
17. Carlson, B. G. and Lathrop, K. D., Transport theory—the method of discrete ordinates. In *Computing Methods in Reactor Physics*, ed. H. Greenspan, C. N. Kelber and D. Okrent. Gordon & Breach, New York, 1968 pp. 171–266.
18. Modest, M. F., *Radiative Heat Transfer*, Chap. 15. McGraw-Hill, New York, 1993.
19. Cengel, Y. A. and Özisik, M. N., Radiation transfer in an anisotropically scattering slab with directional dependent reflectivities. ASME Paper 86-HT-28, 1986.